$In-situ$ monitor of superhydrophobic surface degradation to predict its drag reduction in turbulent flow

Linsheng Zhang (张林生),[1] Colin R Crick,[2] and Robert J Poole[1, a)]

[1)] *School of Engineering, University of Liverpool, Liverpool, L69 3GH, United Kingdom*

[2)] *School of Engineering and Materials Science, Queen Mary University of London, London, E1 4NS, United Kingdom*

(*Electronic mail: robpoole@liverpool.ac.uk)

(Dated: 10 July 2023)

$In-situ$ monitoring is the most insightful technique to examine superhydrophobic surface degradation as it provides real-time information on the liquid-solid interface in a continuous, non-invasive manner. Using reflecting-pixel intensity, we introduced a simple method to characterize $in-situ$ the air-plastron over a superhydrophobic surface in a turbulent channel flow. Prior to the turbulent experiments, a no-flow hydrostatic test was carried out to determine a critical absolute pressure under which the surfaces are able to maintain the air layer for a prolonged period of time. Pressure-drop and velocity measurements were conducted in a series of turbulent flow tests. Resulting from the coupling effects of normal and shear stresses over the plastron, the air layer was progressively lost with flow time which caused the drag ratio (i.e. the friction factor ratio between superhydrophobic and smooth surfaces) to increase. Meanwhile, the average pixel intensity also increased with time and exhibited a consistent trend with the drag ratio evolution. At a fixed near-wall y/h location (within the viscous sublayer), velocity increased with time since the shear stress increased. However, a velocity measurement at the center of the channel exhibited a decrease, consummate with an overall downward shift of the velocity profile. Both pressure-drop and velocity results were observed to be correlated with the average pixel intensities of the images captured over the surfaces and therefore this is a suitable proxy measure of the plastron. This technique is confirmed to be valid for monitoring the air layer and hence predicting the consequent loss of drag reduction.

Superhydrophobic (SHO) surfaces are well known for their drag-reduction properties and a significant number of attempts have been made to modify turbulent flow which is the most common scenario in practical applications[1]. As a shared challenge among these studies[2–4], it is difficult to maintain an air layer/plastron (known as non-wetted Cassie-Baxter state[5]) formed at the liquid-solid interface - which is essential for reducing the frictional drag[6] - upon exposure to a flow. Specifically, in turbulent flow, the air-plastron must suffer from not only high normal stress (pressure) but also shear stresses much higher than laminar flow, which leads to a very quick degradation of the superhydrophobic/drag reduction property[7].

Various optical techniques, including (laser scanning) confocal microscopy[8–12], light/laser scattering[11,13–20], direct (flow) visualization[21–23], have been used to investigate the metastable state of air-plastron and the wetting mode transition (from Cassie-Baxter to Wenzel[24]) under hydrostatic condition[8,19] or in shear flow[12,20]. The increasing hydrostatic pressure deforms the meniscus curvature[12] resulting in a thinner air layer[8]. In a finite time scale, the individual air-plastron would break up (driven by Laplace pressure[9,10]) hence the overall wetting mode of the surface changes to Wenzel[25]. Compared with the hydrostatic condition, a shear flow can alter the mass transfer pattern of air to water at the SHO interface from diffusion-based to force convection dominating[13]. Therefore, the underwater longevity of the air-plastron reduces significantly with an increase of Reynolds numbers/flow rate.[20]. As the flow reaches the turbulent regime, the decay of the air layer is expected to be intensified[13]. However, rarely has research studied the air-plastron longevity in turbulent flow which is directly related to its drag reduction performance[12,23]. In the current study, a simple technique to monitor $in-situ$ the status of the air layer over a superhydrophobic surface in a turbulent channel flow has been introduced and its feasibility has been demonstrated.

Figure 1 demonstrates the working principle for the $in-situ$ air layer monitoring system over the employed superhydrophobic surfaces in a large-scale channel flow facility, which has been previously studied by Agrawal et al[26] and Escudier et al[27] . A schematic representation of the channel system is shown in Figure 1a (see more detail in Section S1 of the Supplementary Materials). A fully developed 2-dimensional turbulent channel flow experiment can be achieved in this rig with dimensions of length(l) $\times$ width(w) $\times$ half-height(h)= $7.2m \times 0.298m \times 0.0125m$, providing an aspect ratio ($AR = w/2h$) of 11.92[28]. A test section (red rectangular highlighted) was installed $6.0m$ downstream ($x/h = 480$) from the inlet. A superhydrophobic coated PVC (polyvinyl chloride, Direct Plastics Limited, UK) substrate with dimensions $100mm$ wide and $200mm$ long (i.e., $8h \times 16h$) was flush mounted at the center of the bottom wall of the test section. The employed SHO materials (SPNC, superhydrophobic polymer-nanoparticle composite) have been recently developed and reported, as discussed in previous studies[29,30]. The detailed fabrication procedure of the current surfaces can be found in Section S2 of the Supplementary Materials. The surface properties were characterized by a dynamic shape analyzer (Kruss, Model DSA 100E) and an optical profiler (WYKO NT1100), and the results are displayed in Table I. The highly water-repellent nature and surface roughness of the current SPNC

[a)] https://www.liverpool.ac.uk/engineering/staff/rob-poole/

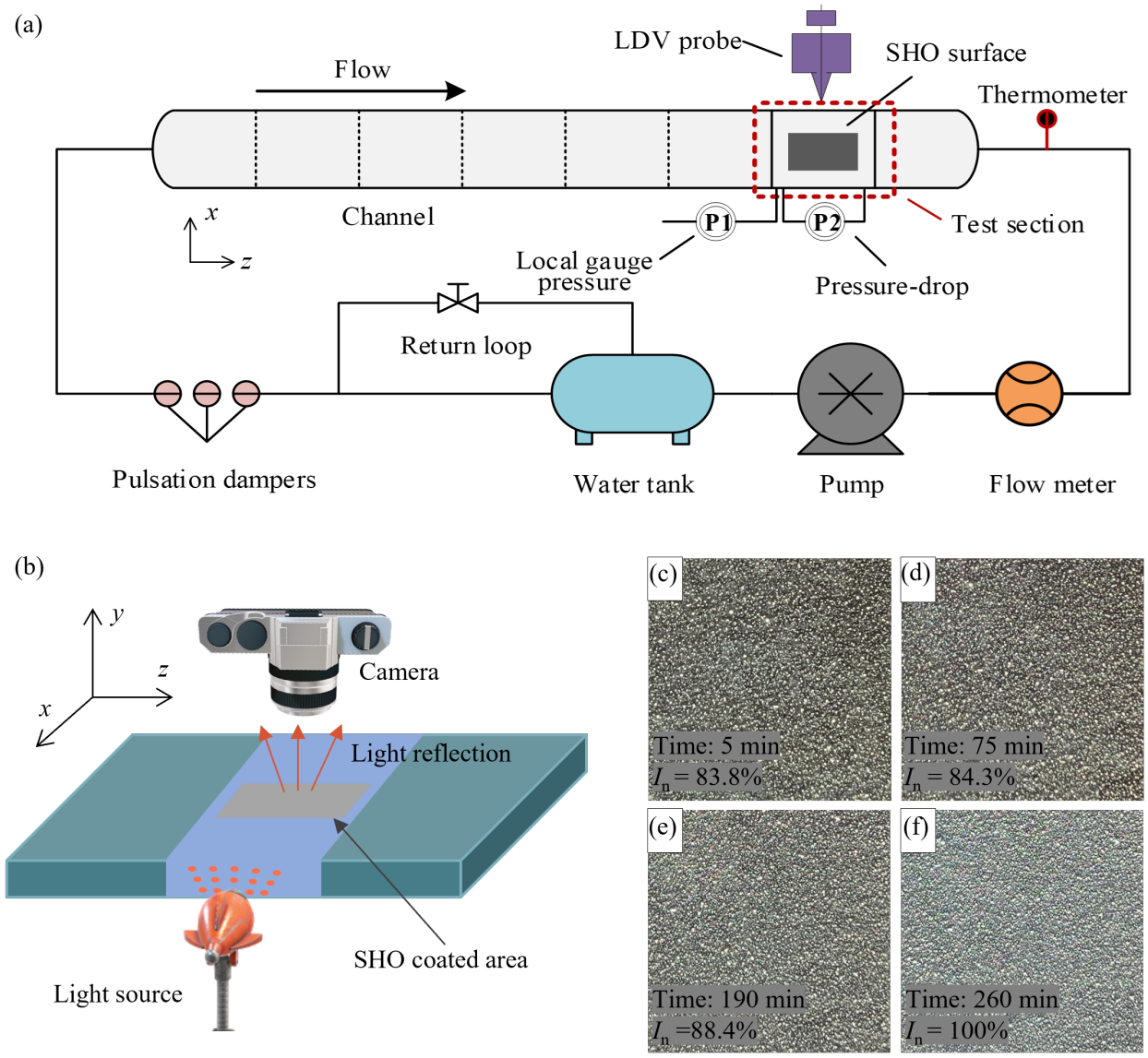

FIG. 1. A simple approach to monitor $in-situ$ the status of the air layer over superhydrophobic surfaces in a turbulent channel flow. (a) Schematic of the channel flow facility used in the current study (not to scale). SHO surface was coated on a PVC substrate (200×100 mm) and fixed under the test section (red highlight) of the channel. (b) Schematic of the real-time image acquisition system over the test section (red highlight in (a)) of the channel. (c) An example for the processed image taken after 5 min of flow, (d) 75 min, (e) 190 min and (f) 260 min. The normalized pixel intensities (I_n) were also displayed below each image.100% normalized intensity represents when the air layer has been lost entirely. This test was undertaken at $Re_h = 1729$ and local gauge pressure P_{gague}=3.58 kPa.

surface has been confirmed, and these advantages are promoted by a dual-layer structure at the microscale level[31]. The side and top walls of the test section are made of borosilicate glass to allow optical access for illuminating light and laser beams. Two pressure transducers were adopted to measure the local gauge pressure (P1, Validyne DP15) 20 mm upstream of the coated area and the pressure-drop (P2, Druck LPX-9381) across a distance of 240 mm over the test surface respectively. Instantaneous streamwise velocity measurement was conducted by a Laser Doppler Velocimetry (LDV) system (Dantec dynamics, see more detail in Section S3 of the Supplementary Materials). In the current study, LDV measurements were carried out at a fixed wall-normal (fixed y/h) location to monitor the time-dependent velocity/turbulent intensity variations. The velocity and RMS (root-mean-square) velocity profile across the channel half-height for a no-slip boundary condition (benchmarked against Direct Numerical Simulation results[32]) are included in the Supplementary Materials (Section S4) to provide a validation of the LDV measurement system. Shown in Figure 1b is the real-time air layer observation setup built at the test section of the channel (highlighted red in Figure 1a). The white light source from the illuminator (Thorlabs OSL2) was reflected by the submerged SHO surface and the formed air layer. The reflection was cap-

TABLE I. Superhydrophobicity and surface roughness characterization of the surface used in the current study (superhydrophobicity was characterized via the dynamic shape analyzer and surface roughness was measured via the optical profiler).

Superhydrophobicity(°)			
Contact angle	Sliding angle	Advancing angle	Receding angle
150.2 ± 3.81	3.87 ± 1.07	152.1 ± 1.6	147.3 ± 2.3
Suface roughness (μm)			
R_a [a]	R_q [b]	R_t [c]	R_z [d]
25 ± 4.6	33 ± 3.3	313 ± 15.8	297 ± 5.4

[a] Average surface roughness.
[b] Root-mean-square surface roughness.
[c] Maximun height of the surface profile.
[d] Average maximum height of the surface profile.

tured as videos/images by a camera (iPhone XR, Apple Inc.) above the channel as illustrated in Figure 1b. The received images were processed (cut to a constant pixel size from the center - 800×800 pixels) by MATLAB software and the average pixel intensity (I) was calculated using Eq.1,

$$I = \frac{1}{N}\sum_{i=1}^{N} I_i \tag{1}$$

in which N is the total number of pixels ($N = 640000$ for each image) and I_i is the intensity of the ith pixel. The average pixel intensity for each image was normalized by the average intensity of the image at the end of each test which refers to the state that an air layer that has been lost entirely (I_{final}),

$$I_n = I/I_{final} \tag{2}$$

in which I_n is the normalized pixel intensity. Four representative images at various time points are displayed in Figures 1c, d, e, and f with the normalized intensity shown below each image. The brightness (reflecting intensity) of the images is observed to increase over time. This phenomenon can be attributed to the dissipation of the air layer (plastron), which reduces the effect of interference (refraction). As a result, the white silica particles which make up a component of the superhydrophobic coatings appear with higher intensity in the captured images. Therefore, the observed increase in average pixel intensity indicates the progressive loss of the air plastron and the diminishing superhydrophobicity with time. At the end of this test, the image was almost purely white, and the normalized pixel intensity reached 100% as no air-plastron survived. Example videos showing the dynamic process of air layer loss are included in the Supplementary Materials (Movie 1 and 2).

We note that the dissolution of the air-plastron occurs even when the surfaces are immersed in quiescent water, especially at very high pressure[8,19]. Therefore, prior to conducting turbulent tests, a "no-flow" hydrostatic test over the employed SHO surface was performed to obtain more understanding of the interaction between the air-plastron and the local absolute pressure. Figure 2 shows the variations of the normalized reflecting pixel intensity as a function of time at various gauge pressures (P_{gauge}) over the surface. In the first 60 min, I_n was increasing with time for all the pressures studied and the higher the pressure the faster the increment. This is primarily due to the thinning of the air layer (i.e., air mass transfer from the plastron to water)[13] so the reflection pixel intensity became higher. From 60 mins to 180 min, the evolution of I_n tends to reach a constant state (thermodynamic equilibrium at the air-water interface[9]) for P_{gauge}=3.65, 4.53 and 5.50 kPa. However, for the other three higher gauge pressures, I_n increased continuously with time and the entire air layer could be lost if the test was long enough (anticipated from the non-zero slope of the curve at the final measurement time). Given this observation, P_{gague}=5.50 kPa was treated as a critical pressure[25] beyond which all the air-plastrons would gradually break up and the wetting mode transforms from Cassie-Baxter to Wenzel. Thus, most of the following turbulent flow experiments were conducted at a $P_{gauge} < 5.50$ kPa so as to keep the local gauge pressure over the test surface below this critical pressure. In this way, the drag reduction decay resulting from air layer loss can be monitored independently. Moreover, the critical pressure (P_{gague}=5.50 kPa) is closely related to the surface topology. According to the Laplace equation (Eq.3), P_{gague} was used to determine the radius of trapped air bubbles (R),

$$\Delta P = \gamma\frac{2}{R} \tag{3}$$

where ΔP represents the pressure difference at the air-water interface. In this case, ΔP is assumed to be equal to P_{gauge}, as we consider the air pressure in the plastron to be constant and equal to atmospheric pressure. $\gamma = 72.4$ mN/m is the surface tension of water in air (note, we measured the actual surface tension of the tap water used in the current study via a surface tensiometer). The estimated length is calculated as 26 μm which is consistent with the average roughness result from surface characterization in Table I.

To confirm the feasibility of the current approach in turbulent flow, pressure-drop measurements were conducted to show the correlation between drag reduction (DR) and I_n. Fanning friction factor ($f = \tau_w/0.5\rho {U_b}^2$) was employed to characterize the drag reduction and calculated by the mean wall shear stress ($\tau_w = \Delta P w h/(l(w+2h))$), in which ρ is the water density, U_b is the bulk velocity and ΔP is the mean pressure-drop across the tested surface. Shown in Figure 3a is a comparison between the calculated friction factor against Re_h ($= \rho U_b h/\mu$, in which μ is the viscosity of water) over reference (smooth) and SHO surfaces in which Pope's correlation is also included[33]. To avoid any potential degradation of the SHO surface, the duration of this pressure-drop measurement is only 1 min in each case. The tests were performed on a single SHO sample and repeated $\sim$3 times. In the Re_h range from 1500-3000, a 5-10% drag reduction is achieved via the current surfaces as shown in Figure 3a. It is noted that at Re_h=4270, there was no drag reduction measured as the friction factor collapsed to the smooth data line. Due to a high local absolute pressure at this Re_h, the air layer over the surface can barely survive to create a slip boundary and therefore no drag-reducing effect was achieved. Focusing on a low Re_h and

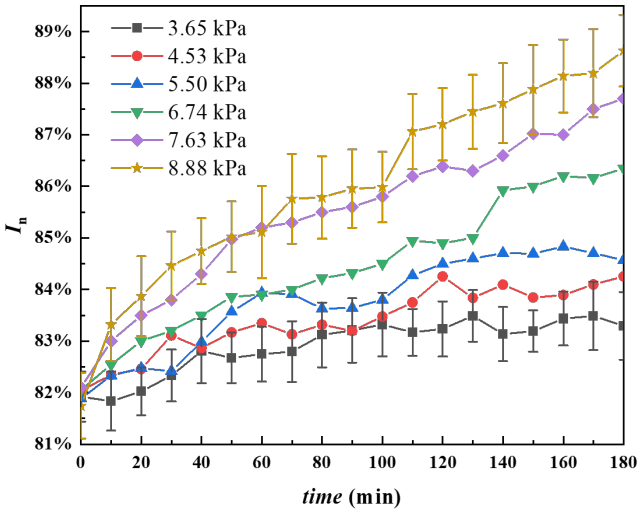

FIG. 2. Variations of the normalized pixel intensity along with time for a no-flow hydrostatic condition. Without starting the pump, this experiment was conducted by increasing the water level of the tank so as to increase hydrostatic pressure over the superhydrophobic samples at the test section. To ensure consistency with the rest of the experiments in this study, the average pixel intensity in this test was normalized by the final average intensity (I_{final}) of the turbulent flow results shown in Figure 3. A 3-hour observation was performed at each pressure and the pressure values in the figure are gauge pressures. Error bars represent the standard deviation of two repeats.

P_{gague}, a long-term pressure-drop measurement was carried out simultaneously with the air layer monitoring ($in-situ$). The drag ratio (f_{SHO}/f_{smooth}, the friction factor ratio between superhydrophobic and smooth surfaces) and normalized intensity (I_n) were plotted as a function of the flow time in Figure 3b. f_{SHO}/f_{smooth} stayed constant in the first 40 min and increased with flow time afterward indicating a time-dependent degradation of the SHO surfaces. Meanwhile, a consistent trend of the normalized intensity showed that the reflecting intensity was increasing because of the loss of air-plastron (transform from Cassie-Baxter to Wenzel state). The loss rate of air-plastron was significantly higher than the hydrostatic case at the same P_{gague} if comparing Re_h=3165 in Figure 3d and P_{gague}=5.50 kPa in Figure 2, for example. Since a turbulent flow was created, the mass transfer from air to water was forced by the viscous and turbulent shear (i.e., the mass transfer pattern changed from dissolution to turbulent forced convection). Although both techniques capture the surface degradation (mostly reversible, see details in Section S6 of the Supplementary Materials), the drag ratio provides quantitative results, and the pixel intensity was more straightforward with a very simple setup. Drag reduction (DR$=1-f_{SHO}/f_{smooth}$) and air-plastron loss ($I_{n,loss}$)) over SHO surfaces against flow time at various Re_h and the corresponding P_{gague} were presented in Figure 3c and d, respectively. $I_{n,loss}$ is a parameter detected from the pixel intensity results and represents directly the level of air-plastron loss, as described in Eq. 4,

$$I_{n,loss}=\frac{I_{final}-I}{I_{final}-I_{initial}} \tag{4}$$

in which $I_{initial}$ is the initial average intensity measured at the start of the test. As discussed, DR decays along with time and a higher gauge pressure would lead to a faster degradation. It is noteworthy that some drag enhancements can be observed at the end of the first 3 tests when the air layer is almost gone. This is attributed to the surface roughness of the SHO sample since there are still peaks and valleys with the maximum size of $\sim$300 μm though the average roughness is as low as 30 μm, as shown in Table. I. Consistency between Figure 3c and d (DR and $I_{n,loss}$) confirms this approach is valid to predict drag reduction of the SHO surfaces qualitatively. Although previous studies have made significant efforts to discuss the influence of hydrostatic pressure and shear stress on superhydrophobic surface degradation, these two parameters have rarely been considered together[12,13,20]. In Figure 3e and f, the drag reduction and air-plastron loss ($I_{n,loss}$) at different P_{gague} but equivalent wall shear stresses (τ_w) are compared. Clearly, the one with high P_{gague} demonstrated a faster superhydrophobic longevity deterioration. Thus, it is clear that the normal and shear force generated from the turbulent flow can independently accelerate the transformation from Cassie-Baxter to Wenzel state for SHO surfaces.

Instantaneous streamwise velocity (u) measurements have been carried out at fixed wall-normal locations (fixed y/h) using the LDV system to obtain information on the local velocity field. Two representative locations were selected to perform the velocity measurement as a function of flow time. At each location velocity samples were collected for 220 min until the surface was unable to produce any drag reduction (air layer dissolved/achieved Wenzel state). Mean velocity ($\overline{u}$) and RMS velocity fluctuations (u') were calculated using the software (BSA flow software) of the LDV system. Shown in Figure 4a is the mean velocity normalized by wall units ($u^+=\overline{u}/u_\tau$) against flow time at two different wall locations (y^+_{final}=3.4 and y^+_{final}=122), in which $u_\tau=\sqrt{\tau_w/\rho}$ is the friction velocity estimated by pressure-drop and y^+_{final} represents the normalized (by wall units) wall locations at the end of the test (the physical spatial location has not changed however the frictional velocity changed due to the loss of the air layer). u^+ at y^+_{final}=3.4 (within the viscous sublayer where the turbulent Reynolds stresses do not significantly contribute to the flow[33]) exhibited an increase along with flow time indicating the wall shear stress was increasing as $\tau_w=\mu(du/dy)$. The air-water contact area decreases due to the dissolution of the air-plastron so the overall shear stress increases. However, a reverse trend of u^+ was observed at y^+_{final} =122 for which the normalized velocity decreased with time to keep mass flow balanced. Thus, it could be expected that the entire velocity profile along the channel height shows a downward shift after the degradation of the surfaces. It is worth pointing out that the value $u'/\overline{u}$ at both locations was constant the whole time, as shown in Figure 4b. This demonstrates that the turbulent intensity was not affected by the SHO surfaces/slip boundary. Figure 4c presents a comparison of the wall shear stress calculated from the near wall velocity ($\overline{u}$ at y^+_{final}=3.4) and the pressure-drop across the SHO surface. Consistent with Figure 4a, the shear stress increased with flow time since the

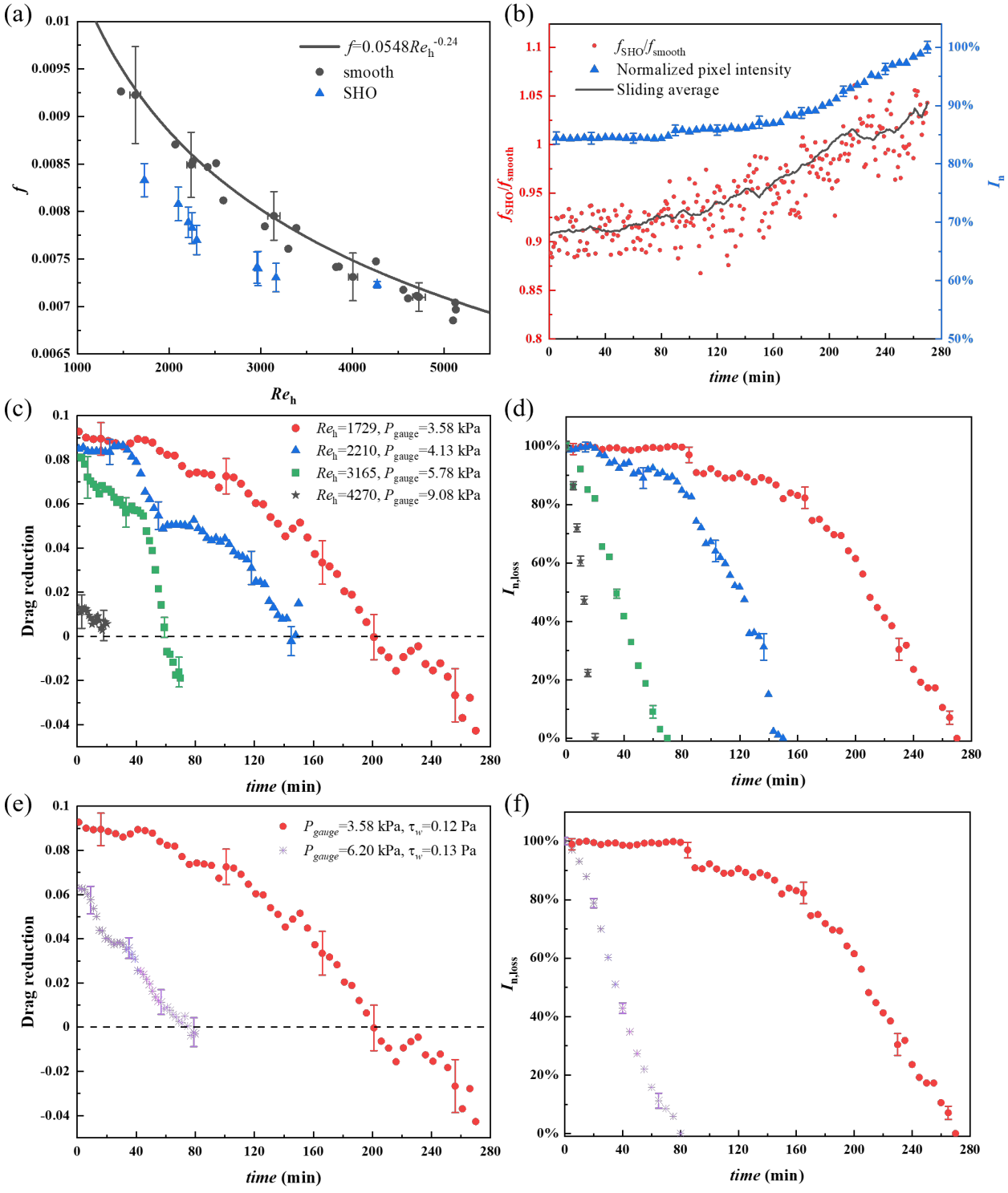

FIG. 3. (a) Fanning friction factor against Reynolds number for both smooth and superhydrophobic surfaces. The correlations from Pope (2000) were also included for reference. (b) Drag ratio (f_{SHO}/f_{smooth}, the friction factor ratio between superhydrophobic and smooth surfaces) against flow time at Re_h =1729 and P_{gague}=3.58 kPa. A sliding average with a period of 30 data-points was applied to present a clear trend from the high fluctuations. (c) Drag reduction and (d) air-plastron loss (also indicated as intensity increase previously) against flow time at various Reynolds numbers and gauge pressures. Comparison of the drag reduction (e) and air-plastron loss (f) for the same shear stress but different gauge pressures. Drag reduction results in (a) and (e) were simplified by applying a sliding average from the original data. Labels in (d) and (f) are the same as those in (c) and (e). Error bars represent the standard deviation of the repeats.

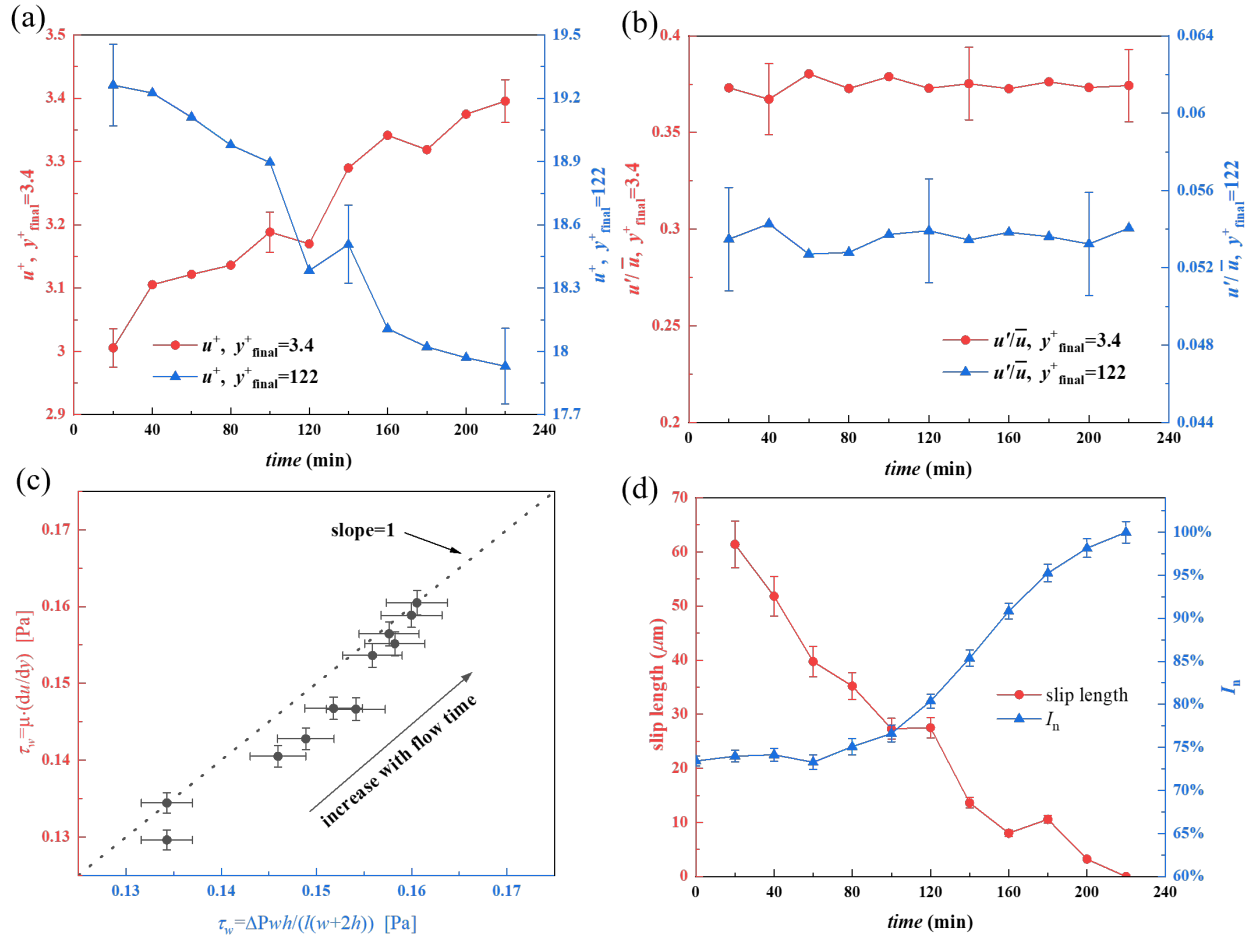

FIG. 4. Long-term LDV measurement over superhydrophobic surfaces at fixed wall-normal locations. (a) Mean streamwise and (b) RMS (root-mean-square) velocities against flow time at the near wall location (viscous sublayer, y^+_{final}=3.4) and channel center (outer layer, y^+_{final}=122). The mean velocity was normalized by the inner scale and the RMS velocity was normalized by the mean velocity. Error bars were determined by the relative uncertainties of the mean velocity (2-3%) and turbulent intensity (4-6%). (c) Comparison between the wall shear stress calculated from near-wall velocity measurements and pressure-drop results. The error bars for $\tau_w = \mu(du/dy)$ were determined by the error of the velocity and the wall distance. However, error bars of $\tau_w = \Delta P wh/(l(w+2h))$ were determined by the uncertainty of the pressure transducer.(d) Slip-length and normalized pixel intensity against flow time. The uncertainty of slip length was estimated by the error of the velocity and wall distance.This LDV measurement was performed at P_{gauge}=3.89 kPa.

air-plastron was being lost. Moreover, these two calculations were almost equal with a very slight shift downwards to the right (τ_w was slightly higher estimated from ΔP). This could be attributed to the pressure-drop being measured at a cross-sectional area in which only 13.7% was actually coated as SHO so that the shear stress was over-estimated. Lastly, in Figure 4d, the slip length (b) estimated by the near wall velocity (using Eq.5) was plotted versus flow time,

$$\mu \frac{du}{dy}\bigg|_{\text{no-slip}} = \mu \frac{du}{d(y-b)}\bigg|_{\text{slip}} \tag{5}$$

Note that the maximum slip length result here (62.5 μm) is less than half of the results we measured in the previous study using the same SHO surface (which was above 140 μm) in a laminar flow via a rheometric device[34]. This is mainly because of the significantly higher absolute pressure that limits the initial plastron thickness of the current surface. The decay of slip length illustrated the degradation of SHO surfaces. Similar results have been also reported using different SHO surfaces in a rheometer-based laminar flow[35]. However, the normal stress (pressure) was much lower so it took $\sim$ 8 hours for the sample to lose all superhydrophobicity. As an additional indicator, the normalized pixel intensity (I_n) in Figure 4d also demonstrates the SHO surface degradation though the sensitivity is low at the beginning of the test.

To sum up, a simple technique to monitor $in-situ$ the air layer over superhydrophobic surfaces in turbulent channel flow was introduced with a very simple apparatus. The requirements are only a basic light source and a small camera (e.g. phone camera), without the need for any laser or PC during the test procedure. This study demonstrated the feasibility of this technique to reflect the drag reduction and air layer sta-

tus of a SHO surface via both global pressure-drop across the sample and local velocity at different wall locations. Furthermore, the effect of normal and shear stresses on the longevity of air-plastron was individually studied. For a given SHO surface (with specific surface geometry), a critical hydrostatic pressure should be determined under which the surface is able to maintain the air layer for a long time. Finally, it is found that in turbulent flow the current surface would lose all its air layer and drag reduction ability within a few hours under the coupling effects of normal and shear stresses. Since a large-scale channel flow facility was adopted, the lifetime of the air layer is relatively short under the impact of significantly high gauge pressures. However, these scenarios are more realistic and technically important considering the real-world drag reduction application of SHO surfaces.

SUPPLEMENTARY MATERIAL

See the supplementary material (PDF) for the description of the channel flow facility, the fabrication of superhydrophobic surfaces, the setup of laser Doppler velocimetry, the LDV results at no-slip boundary condition, the evaluation of the permanent degradation of the employed surfaces, the MATLAB code for the image processing as well as the repeat tests at $Re \approx 3000$. In addition, two representative videos (Movie 1 and 2) for the dynamic process of air plastron loss are also available.

ACKNOWLEDGMENTS

Linsheng Zhang acknowledges the financial support from the joint scholarship of China Scholarship Council and the University of Liverpool. The authors would also like to thank Prof. Geoff Dearden and Mr. Yin Tang for their generous help with the optical profilometer. Dr. Henry Ng is also thanked for useful comments on the draft manuscript.

AUTHOR DECLARATIONS

Conflict of Interest

The authors have no conflicts to disclose.

Author Contributions

Linsheng Zhang: Methodology(equal); Software(lead); Visualization (lead), Writing-Original Draft Preparation (lead). Colin R Crick: Conceptualization (supporting); Methodology (equal); Resources (equal); Writing-Review & Editing (supporting). Robert J Poole: Conceptualization (lead); Methodology (equal); Supervision (lead); Resources (equal); Writing-Review & Editing (lead).

DATA AVAILABILITY STATEMENT

The data that support the findings of this study are available from the corresponding authors upon reasonable request.

REFERENCE

[1]H. Park, C.-H. Choi, and C.-J. Kim, "Superhydrophobic drag reduction in turbulent flows: a critical review," Experiments in Fluids **62**, 1–29 (2021).
[2]E. Aljallis, M. A. Sarshar, R. Datla, V. Sikka, A. Jones, and C.-H. Choi, "Experimental study of skin friction drag reduction on superhydrophobic flat plates in high reynolds number boundary layer flow," Physics of fluids **25**, 025103 (2013).
[3]P. Du, J. Wen, Z. Zhang, D. Song, A. Ouahsine, and H. Hu, "Maintenance of air layer and drag reduction on superhydrophobic surface," Ocean Engineering **130**, 328–335 (2017).
[4]Z. Wang, J. Ji, Y. Guo, T. Tao, X. Hu, Y. Zhu, X. Liu, K. Liu, and Y. Jiao, "Robust air cavity generation on sacrificial microstructures for sustainable underwater drag reduction," Applied Physics Letters **121**, 181602 (2022).
[5]A. Cassie and S. Baxter, "Wettability of porous surfaces," Transactions of the Faraday society **40**, 546–551 (1944).
[6]J. P. Rothstein, "Slip on superhydrophobic surfaces," Annual review of fluid mechanics **42**, 89–109 (2010).
[7]J. W. Gose, K. Golovin, M. Boban, J. M. Mabry, A. Tuteja, M. Perlin, and S. L. Ceccio, "Characterization of superhydrophobic surfaces for drag reduction in turbulent flow," Journal of Fluid Mechanics **845**, 560–580 (2018).
[8]P. Lv, Y. Xue, Y. Shi, H. Lin, and H. Duan, "Metastable states and wetting transition of submerged superhydrophobic structures," Physical review letters **112**, 196101 (2014).
[9]P. Papadopoulos, L. Mammen, X. Deng, D. Vollmer, and H.-J. Butt, "How superhydrophobicity breaks down," Proceedings of the National Academy of Sciences **110**, 3254–3258 (2013).
[10]R. Poetes, K. Holtzmann, K. Franze, and U. Steiner, "Metastable underwater superhydrophobicity," Physical review letters **105**, 166104 (2010).
[11]T. Verho, J. T. Korhonen, L. Sainiemi, V. Jokinen, C. Bower, K. Franze, S. Franssila, P. Andrew, O. Ikkala, and R. H. Ras, "Reversible switching between superhydrophobic states on a hierarchically structured surface," Proceedings of the National Academy of Sciences **109**, 10210–10213 (2012).
[12]Y. Xiang, Y. Xue, P. Lv, D. Li, and H. Duan, "Influence of fluid flow on the stability and wetting transition of submerged superhydrophobic surfaces," Soft Matter **12**, 4241–4246 (2016).
[13]B. V. Hokmabad and S. Ghaemi, "Effect of flow and particle-plastron collision on the longevity of superhydrophobicity," Scientific reports **7**, 1–10 (2017).
[14]D. Dilip, M. Bobji, and R. N. Govardhan, "Effect of absolute pressure on flow through a textured hydrophobic microchannel," Microfluidics and Nanofluidics **19**, 1409–1427 (2015).
[15]M. S. Bobji, S. V. Kumar, A. Asthana, and R. N. Govardhan, "Underwater sustainability of the "cassie" state of wetting," Langmuir **25**, 12120–12126 (2009).
[16]Y. Wang, B. Zhang, H. Dodiuk, S. Kenig, C. Barry, J. Ratto, J. Mead, Z. Jia, S. Turkoglu, and J. Zhang, "Effect of protein adsorption on air plastron behavior of a superhydrophobic surface," ACS Applied Materials & Interfaces **13**, 58096–58103 (2021).
[17]L. Lei, H. Li, J. Shi, and Y. Chen, "Diffraction patterns of a water-submerged superhydrophobic grating under pressure," Langmuir **26**, 3666–3669 (2010).
[18]M. A. Samaha, F. O. Ochanda, H. V. Tafreshi, G. C. Tepper, and M. Gad-el Hak, "In situ, noninvasive characterization of superhydrophobic coatings," Review of Scientific Instruments **82**, 045109 (2011).
[19]M. Xu, G. Sun, and C.-J. Kim, "Infinite lifetime of underwater superhydrophobic states," Physical review letters **113**, 136103 (2014).
[20]M. A. Samaha, H. V. Tafreshi, and M. Gad-el Hak, "Influence of flow on longevity of superhydrophobic coatings," Langmuir **28**, 9759–9766 (2012).

[21]P. Forsberg, F. Nikolajeff, and M. Karlsson, "Cassie–wenzel and wenzel–cassie transitions on immersed superhydrophobic surfaces under hydrostatic pressure," Soft Matter **7**, 104–109 (2011).
[22]P. R. Jones, X. Hao, E. R. Cruz-Chu, K. Rykaczewski, K. Nandy, T. M. Schutzius, K. K. Varanasi, C. M. Megaridis, J. H. Walther, P. Koumoutsakos, *et al.*, "Sustaining dry surfaces under water," Scientific reports **5**, 12311 (2015).
[23]D. Moreira, S.-h. Park, S. Lee, N. Verma, and P. R. Bandaru, "Dynamic superhydrophobic behavior in scalable random textured polymeric surfaces," Journal of Applied Physics **119**, 125302 (2016).
[24]R. N. Wenzel, "Resistance of solid surfaces to wetting by water," Industrial & Engineering Chemistry **28**, 988–994 (1936).
[25]B. Liu and F. F. Lange, "Pressure induced transition between superhydrophobic states: Configuration diagrams and effect of surface feature size," Journal of colloid and interface science **298**, 899–909 (2006).
[26]R. Agrawal, H. C.-H. Ng, E. A. Davis, J. S. Park, M. D. Graham, D. J. Dennis, and R. J. Poole, "Low-and high-drag intermittencies in turbulent channel flows," Entropy **22**, 1126 (2020).
[27]M. P. Escudier, A. K. Nickson, and R. J. Poole, "Turbulent flow of viscoelastic shear-thinning liquids through a rectangular duct: Quantification of turbulence anisotropy," Journal of non-newtonian fluid mechanics **160**, 2–10 (2009).
[28]R. B. Dean, "Reynolds number dependence of skin friction and other bulk flow variables in two-dimensional rectangular duct flow," Journal of fluid engineering **100**, 215–223 (1978).
[29]R. L. Upton, Z. Davies-Manifold, M. Marcello, K. Arnold, and C. R. Crick, "A general formulation approach for the fabrication of water repellent materials: how composition can impact resilience and functionality," Molecular Systems Design & Engineering **5**, 477–483 (2020).
[30]Y. A. Mehanna and C. R. Crick, "Image analysis methodology for a quantitative evaluation of coating abrasion resistance," Applied Materials Today **25**, 101203 (2021).
[31]S. F. Ahmadi, V. Umashankar, Z. Dean, B. Chang, S. Jung, and J. B. Boreyko, "How multilayered feathers enhance underwater superhydrophobicity," ACS Applied Materials & Interfaces **13**, 27567–27574 (2021).
[32]J. Kim, P. Moin, and R. Moser, "Turbulence statistics in fully developed channel flow at low reynolds number," Journal of fluid mechanics **177**, 133–166 (1987).
[33]S. B. Pope, *Turbulent flows* (Cambridge university press, 2000).
[34]L. Zhang, Y. A. Mehanna, C. R. Crick, and R. J. Poole, "Surface tension and viscosity dependence of slip length over irregularly structured superhydrophobic surfaces," Langmuir **38**, 11873–11881 (2022).
[35]H. Xu, C. R. Crick, and R. J. Poole, "Evaluating the resilience of superhydrophobic materials using the slip-length concept," Journal of Materials Chemistry A **6**, 4458–4465 (2018).